The 2013, Mw 7.7 Balochistan Earthquake, seismic slip boosted on a misoriented fault

Jean-Philippe Avouac[a,*], Francois Ayoub[a], Shengji Wei[a], Jean-Paul Ampuero[a], Lingsen Meng[a], Sebastien Leprince[a], Romain Jolivet[a], Zacharie Duputel[a] and Don Helmberger[a]

[a] Geology and Planetary Science Division, Caltech Institute of Technology, Pasadena, USA

* Corresponding Author (avouac@gps.caltech.edu)

ABSTRACT

We analyse the Mw 7.7 Balochistan earthquake of 09/24/132013 based on ground surface deformation neasured from sub-pixel correlation of Landsat-8 images, combined with back-projection and finite source modeling of teleseismic waveforms. The earthquake nucleated at the southern tip of the Chaman strike-slip fault and propagated southwestward along the Hosbah fault at front of the Kech Band. The rupture was mostly unilateral, propagated at a speed of 3km/s on average and produced a 200km surface fault trace with purely strike-slip displacement peaking to 10m and averaging around 6m. The finite source model shows that slip was maximum near the surface. Although the Hosbah fault is dipping by 45° to the North, in accordance with its origin as a thrust fault within the Makran accretionnary prism, slip was nearly purely strike-slip during that earthquake. Seismic slip on such a misoriented fault was possibly boosted due to the influence of the free surface on dynamic stresses or to particular properties of the fault zone. Strike-slip faulting on thrust fault within the eastern Makran is interpreted as due to eatsward extrusion of the accretionnary prism as it bulges out over the Indian plate. The Makran megathrust and the Chaman fault system have been brought closer to failure by this earthquake.

1. Introduction

The Mw 7.7 Balochistan earthquake which occurred in southwestern Pakistan on 09/24/13 nucleated at the southern tip of the Chaman fault, which is part of the 1200 km long left-lateral fault system accomodating the 3 cm/yr northward motion of the western side of India relative to Eurasia (Lawrence R.D. et al., 1981; Szeliga et al., 2012) (Figure 1). The moment tensor (Figure 1) indicates purely strike–slip motion on the 45° North dipping fault plane and a slight non-double component suggestive of a non-planar fault geometry. The fault trace determined in this study (Figure 2) shows that the rupture indeed bends westward to merge with the arcuate tectonic fabric of the eastern Makran accretionary prism. These observations demonstrate the rupture of a strongly mis-oriented fault: Anderson's theory would require either purely dip-slip motion on the 45° dipping fault or strike-slip motion on a vertical fault. This event thus sheds some interesting new light on the infuence of fault geometry on seismic ruptures.

In this study, we first characterize and model the source of the earthquake combining remote-sensing and seismological observations. We nest discuss the implications for earthquake dynamics and the tectonic significance of that event.

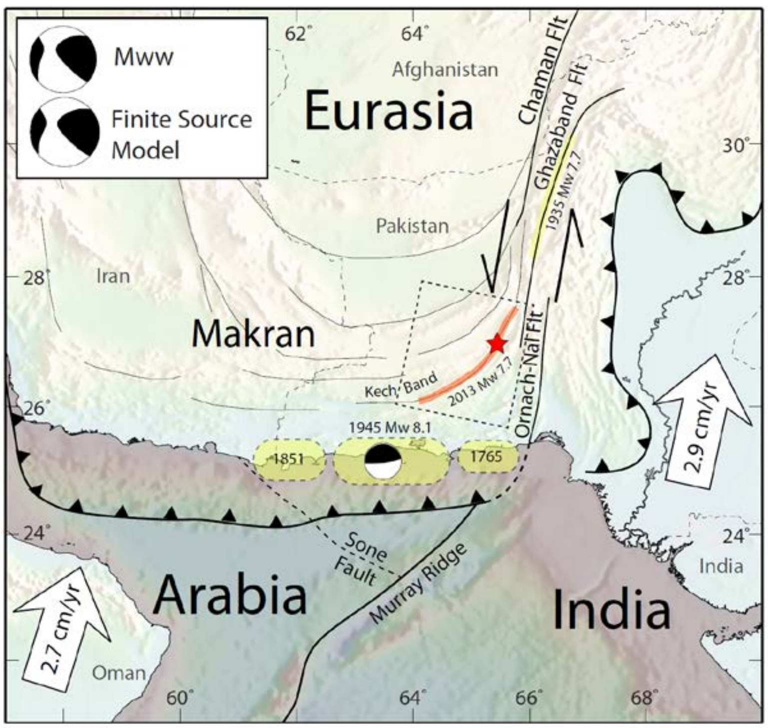

Figure 1: Seismotectonic setting of the September 24, 2013, Mw 7.7 Balochistan earthquake. *The location of the epicenter, red star* (http://earthquake.usgs.gov/earthquakes/eventpage/usb000jyiv)*, shows that the earthquake nucleated at the southern tip of the Chaman fault, the major left-lateral strike-slip fault accommodating the northward motion of India relative to Eurasia. The curved trace of the surface rupture shows that the earthquake propagated along a restraining fault bend within the Makran accretionnary prism. The box shows the footprint of Figure 2. The W-phase moment tensor determined (inset) shows purely strike motion on the fault plane sub-parallel to the observed fault trace (see Supplements). The 10% non-double component is consistent with the curved geometry of the fault trace. The moment tensor of the finite source model (also in inset) is nearly identical to the W-phase moment tensor. Tectonic setting based on the literature(Byrne et al., 1992; Kukowski et al., 2000; Lawrence R.D. et al., 1981). Arrows show the Arabia (Reilinger et al., 2006) and India (Ader et al., 2012) plate motions relative to stable Eurasia.*

2. Optical image correlation results

We measured horizontal surface displacements induced by the earthquake from cross-correlation of optical images using the COSI-Corr technique (Leprince et al., 2007) (see Supplements for details). We used images from Landsat-8, which is an optical satellite system, launched by NASA in February 2013 and now operated by the USGS, which images the earth every 16 days. We processed two adjacent pairs of images along the satellite track. The pre-earthquake images were acquired on September, 10, 2013 (14 days before the event), and post-earthquake images were acquired on September, 26, 2013 (2 days after the event). We correlated the panchromatic band (band 8), which has a ground sampling distance of 15 m, using a window size of 64x64 pixels (960x960 m) and a sliding step of 16 pixels (240 m). The procedure yields the surface displacement vector fields with a ground sampling distance of 240 m, close to the actual resolution of the measurements, with a 1-σ uncertainly of 30 cm. The results from the correlating the two pairs were corrected for CCD-arrays artifacts and mosaicked as described in the supplements.

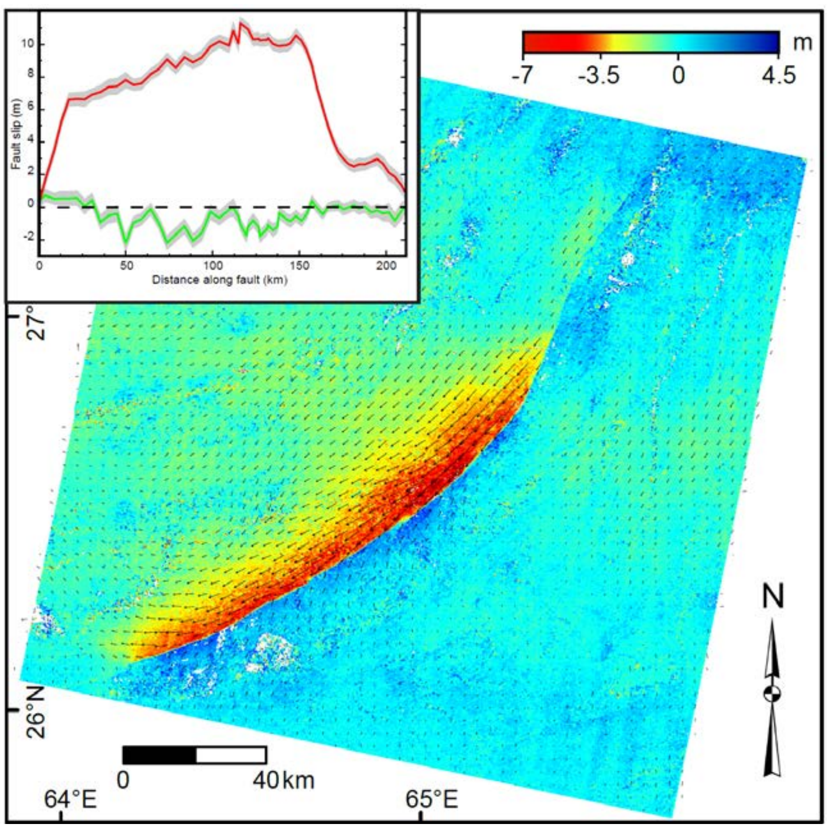

Figure 2: Surface displacement measured from cross-correlation of optical satellite images. *We used two pairs of Landsat 8 images (15m GSD), acquired on 09/10/13 and 09/26/13, which were*

co-registered and correlated using COSI-Corr(Leprince et al., 2007). Vector field show horizontal displacements and color shading shows the EW component of the displacement field (positive eastward) calculated with a 64x64 pixel correlation window and a 240 m Ground Sampling Distance (GSD). The 1-σ uncertainty on EW and NS displacement is estimated to 0.47 m and 0.60 m, respectively (see Supplements). Inset: Surface fault slip measured from the displacement discontinuity across the fault trace; red shows strike-slip component (positive for left-lateral) and green fault-normal component (positive for extension). See Supplement for details.

These measurements (Figure 2) reveal a 200 km long continuous surface rupture following the Hosbah thrust fault(Lawrence R.D. et al., 1981) which runs along the front of the the Kech Band, a mountainous ridge peaking to about 1200 m. Fault slip is essentially strike-slip, 6 m on average, and reaches up to 10 m. The fault-normal component indicates a very small thrust component consistent with the restraining bend geometry. Displacements are significantly larger on the northwestern side than on the southeastern side of the fault. This asymmetry clearly indicates a northwest dipping fault consistent with the W-phase moment tensor.

3. Backprojection results

We imaged the rupture process by back-projecting (Ishii et al., 2005) teleseismic P waves recorded by the Japanese Hi-net seismic network using the Multitaper-MUSIC array processing technique (Meng et al., 2011) (Figure 3). The technique tracks the spatio-temporal evolution of the sources of radiation in the 0.5-2 Hz frequency band during the rupture process. Source radiation is reliably imaged during 50 s indicating southwestward unilateral rupture with speed fluctuating around 3 km/s on average. The distribution of the high frequency radiators relative to the mainshock's epicenter follows remarkably well the fault geometry derived from the optical images. The high frequency radiations amplified as the rupture propagated southwestwards.

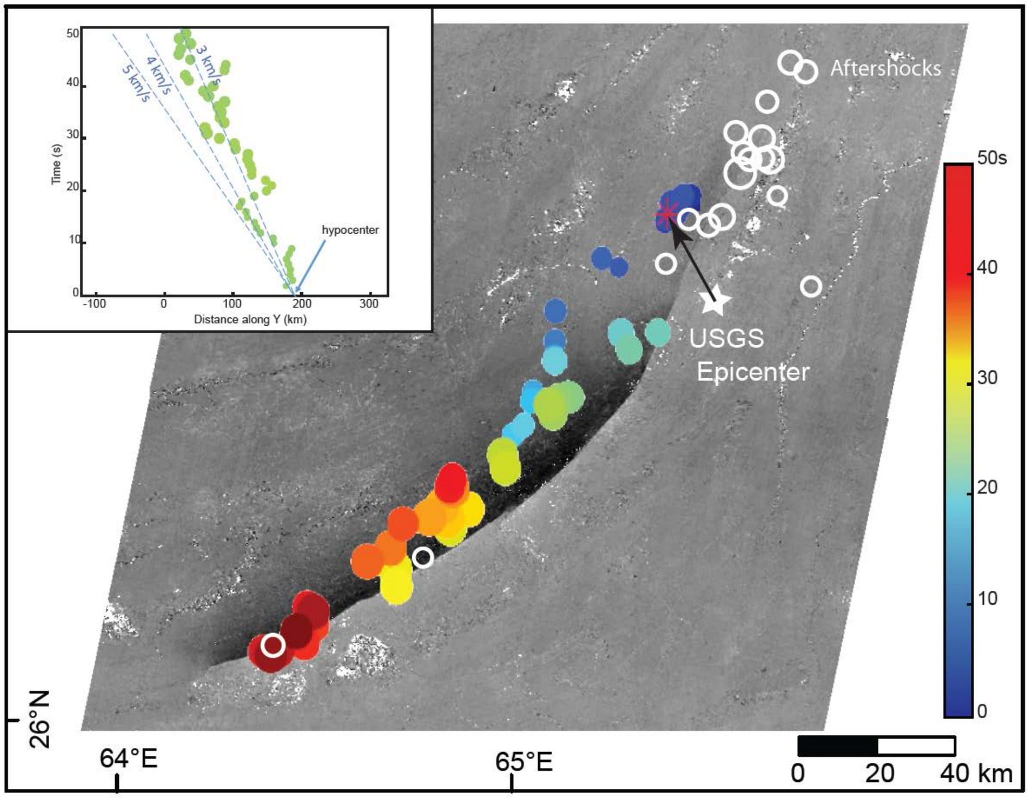

Figure 3: Rupture kinematics from backprojection of teleseismic waves. *Rupture process imaged from back-projection of teleseismic P waves recorded by the Japanese seismic network using the Multitaper-MUSIC array processing technique(Meng et al., 2011). Color dots show the locations of the high frequency sources (frequency band: 0.5-2Hz). Size is proportional to the beamforming amplitude and color indicates the time of each window center relative to hypocentral time. The sliding window duration is 10s and the first window is centered on first P waves arrival. Inset shows timing of the high frequency sources plotted as a function of distance along the fault indicate westward unilateral rupture with average speed of about 3 km/s, close to the estimated S-waves velocity in the depth range of the rupture (Table S1). White circles show aftershocks with mb>4 over the first week following the mainshock (NEIC catalogue).*

4. Finite source Modeling

We next determined a finite source kinematic model of the rupture from the joint inversion of the surface displacements and of seismic waveforms in the 0.01-1 Hz frequency band using the technique of Ji et al. (2002) (see Supplements for details). We approximate the fault geometry with six planar fault segments. Dip angles were adjusted by trial and error. The model assumes that the rupture consists of a propagating rupture front with slip accruing in the wake of the rupture front over a duration called the rise-time. The back-projection results lend support to the relevance of that formalism, which has also been shown to be adapted to retrieve dynamic ruptures models for a variety of scenarios(Konca et al., 2013). For each subfault, we solve for the slip amplitude and rake, rise time and rupture velocity. We assume that all of the measured slip at the surface occurred during the seismic phase, ignoring the possibility of afterslip over the two days following the earthquake. The finite-source model (Figure 4) shows that the rupture initiated on a sub-vertical subfault and then propagated to the southwest on 45°dipping fault segments releasing a cumulative moment of 5.4 10^{21} N.m, corresponding to a moment magnitude Mw 7.75. The moment tensor computed by summing the moment tensors from all subfaults is found to be nearly identical to the W phase moment tensor (Figure 1, inset). In particular, our model does correctly account for the non double-couple component determined by the point source solution. In our model, most of the slip occurred at depth shallower than 15 km. The total duration is about 60 s and the rupture velocity is quite uniform around 3 km/s on average. This value is consistent with the best fitting rupture velocity obtained for inversions run with a constant rupture velocity (Figure 4). The rake is everywhere close to zero, showing nearly purely strike-slip motion. Rise-times are generally less than 8 s, much shorter than the total duration of the source, indicating a clear pulse-like rupture (Heaton, 1990). Rise-time (see Supplements) approximately scale with slip, indicating a fault slip rate of about 1 m/s throughout the rupture. Note that the peak slip rate could be much larger as our model does not resolve high frequencies (due to the filtering of frequency below 1 Hz and the smooth assumed slip-rate function). The average stress drop derived from the released seismic moment and surface rupture area is 3.3 MPa.

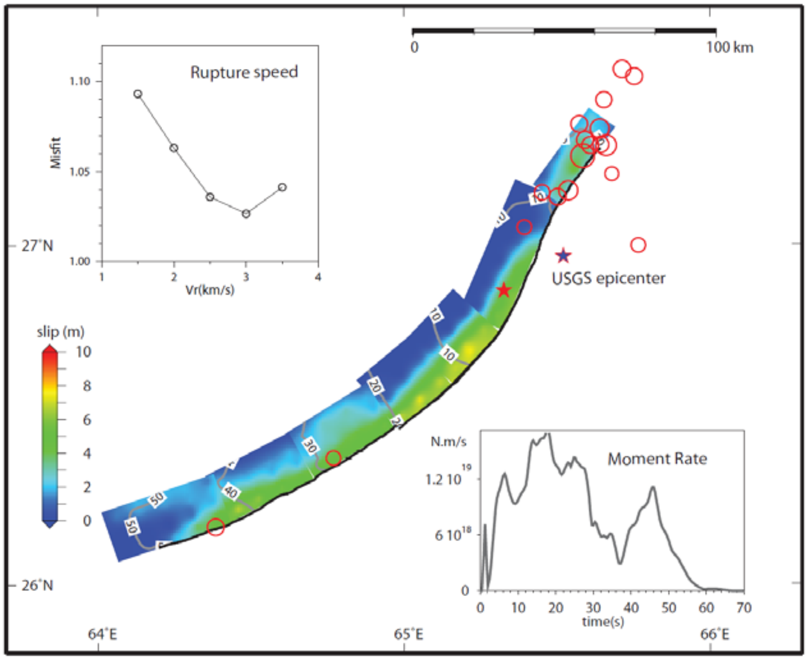

Figure 4: Finite source kinematic model. *Slip distribution in map view with isochrons (in seconds) of the rupture front propagation determined from the joint inversion of the surface displacements and teleseismic waveforms. The average speed of the rupture is 3 km/s for this preferred model. Red circles show aftershocks with mb>4. over the first week following the mainshock (NEIC catalogue). Lower inset shows the moment rate function corresponding to this model. Upper inset shows the sensitivity to the rupture speed determined by running inversions with an imposed constant rupture speed. The best fitting model is obtained for a rupture speed of 3 km/s, close to the average value of our preferred model, and close to the estimated S-waves velocity in the depth range of the rupture (Table S1).*

5. Discussion

5.1 regional tectonic interpretation

This study demonstrates that, while the earthquake nucleated on a fault segment close to being optimally oriented, it was able to propagate for over 150 km along severely misoriented fault segments, most probably preexisting thrust faults within the Makran accretionary prism. Structural field investigations suggest that the thrust faults within the prism cut through Paleogene to Early Miocene turbidites detached from the underthrusting oceanic Arabian plate (Ellouz-Zimmermann et al., 2007). The basal decollement lies at a depth probably larger than 12 km beneath the Kech band (Ellouz-Zimmermann et al., 2007). This is consistent with our finding that most of the slip occurred at depth shallower than 15 km. Actually strike-slip striations on some thrust faults in the eastern Makran have been observed in the field, and were ascribed to strike-slip faults branching into these thrust faults (Platt et al., 1988), as actually happened during the 2013 earthquake.

These preexisting thrust faults were reactivated with nearly purely strike-slip motion although kinematic compatibility with purely strike-slip motion on the North-South trending Chaman fault would have required significant thrusting. The thrusting component is very minor but does attest to a compressional regime.

It is interesting to comment on how the 2013 Balochistan earthquake relates to the regional tectonic setting. A recent geodetic study (Szeliga et al., 2012) noticed that the geodetic strain is not centered on the Chaman fault system (the Chaman, Gazaband and Ornach-Nal faults, Figure 1), but offseted to the West. It is thus possible that a fraction of the wrench motion between the Makran and Peninsular India is accomodated by faults within the eastern Makran such as the ones which were activated in 2013. However strike-slip faulting along the Hosbah fault cannot play an important role in accomodating the India-Eurasia relative motion given its strike. Similarly, the obliquity of the Arabia/Eurasia convergence is probably too small to explain a significant eastward motion of of the outer portion of the eastern Makran prism, especially as it is dimished by right-lateral shear across the Sone fault offshore Makran (Kukowski et al., 2000). A possible interpratation is that the outer part of the prism is extruded eastward as is it squeezed against the Helmand block, which is the cratonic block forming the backstop of eastern Makran (Figure 5). As a resust the prism bulges outward and is thrust over the India basement east of the Chaman fault system. The Chaman fault system propagates southwards across the extruded portion of the prism. The arcuate shape of the fold-and-thrust belts in eastern the Makran and the N-S to NW-SE trending formal faults noticed by Lawrence et al. (1981), which are actually prominent in the morphology, would have developed as the folds are dragged and stretched due to left-lateral shear along the Chaman Fault system (Figure 5).

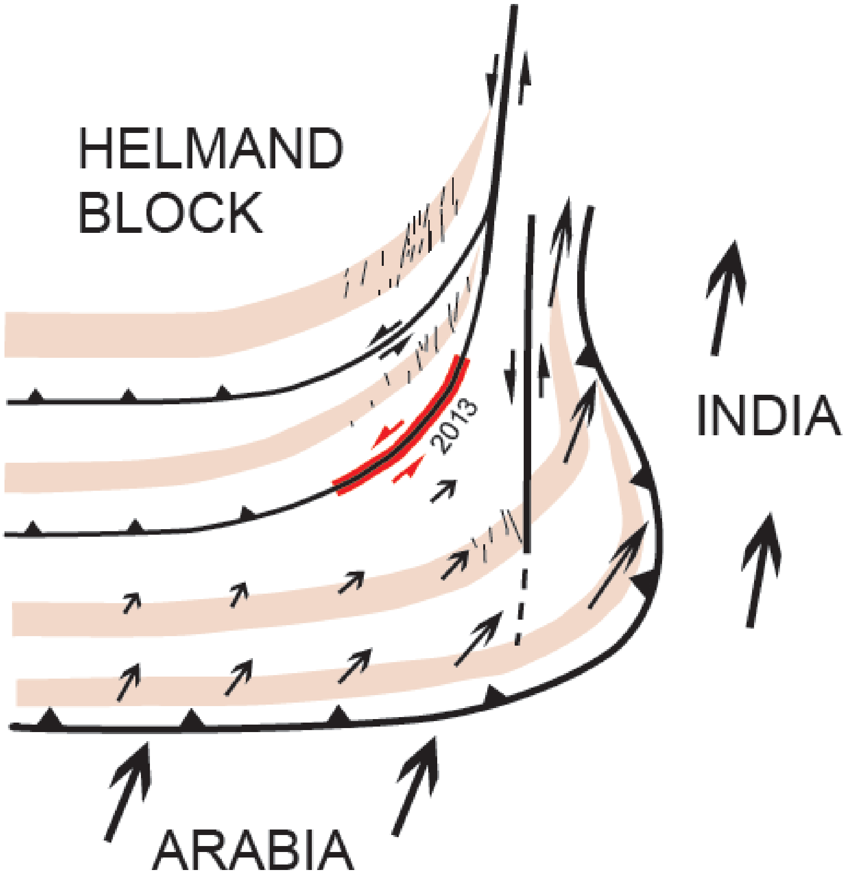

Figure 5: Possible interpretation of regional tectonics. *Sketch of faults pattern based on Lawrence et al (1981). Thin N-S trending line represents normal faults. Vectors show long term velocities relative to Iran assuming that a fraction of the oblique convergence between Arabia and central Iran is absorbed within the Makran accretionnary wedge. The fold-and-thrust belts within the Makran are dragged and stretched due to left-lateral shear along the Chaman Fault system. The eastern part of the wedge is squeezed out and bulges eastwards.*

5.3 Implications for seismicity on the Chaman fault and Makran megathrust

The 2013 earthquake was unable to propagate along the Chaman fault which is yet better oriented than the Hosbah fault (Figure 2). It is also paradoxical that most of the aftershocks actually clustered along the Chaman fault, northwards of the epicenter, despite the southwestward directivity of the rupture. The 2013 earthquake must have brought the Chaman fault closer to yielding, as the aftershocks indicate, enhancing the probability that it ruptures in a significant seismic event. Historical seismicity on the Chaman fault is actually remarkably low (Ambraseys, 2003; Szeliga et al., 2012) in view of its length, longer than 1000 km and faster than 2 cm/yr slip rate. There are only four significant earthquakes reported on that fault system over the last 500 years. The major one is the Mw 7.5 Quetta earthquake which probably ruptured the Ghazaband fault in 1935. The oher ones, which occurred in 1505, 1892 and 1975, are more moderate with magnitudes between 6 and 7. This would suggest that either aseismic creep plays a large role in accomodating the long term slip rate on that fault or that the largest earthquakes are not represented in historical seismicity.

The sparse geodetic data available do indicate low interseismic coupling (Szeliga et al., 2012) so that it is tempting to advocate for aseismic creep to explain the fact that the rupture didn't propagate nortwards and the generaly low level of seismicity on the Chaman fault.

The data coverage is however too sparse to draw any firm conclusion about the propotion of aseismic creep and the potential presence of an aseismic barrier (Kaneko et al., 2010) north of the epicenter.

The Makran Megathrust must also have been brought locally closer to failure following the 2013 Balochistan earthquake. This megathrust has produced large tsunamigenic earthquakes in the past, notably in 1945 (Byrne et al., 1992) (Figure 1), and it might have the potential to generate even larger earthquakes (Smith et al., 2013). Unfortunately, this discussion is very speculative as the sparsity of geodetic mesurements prevents assessing precisely the rate at which elastic strain is buidling up in preparation of a future earthquake on those two plate boundaries.

5.3 Boosted slip at shallow depth on misoriented fault, implications for faults dynamics

Fault geometry determines the initial stress prior to an earthquake as well as the dynamic stresses during the seismic rupture (Kase and Day, 2006). It is therefore recognized as one of the major factors governing the nucleation and propagation of seismic ruptures. Observations (Bouchon et al., 1998; Bouchon et al., 2000; King and Nabelek, 1985) and numerical simulations(Bouchon and Streiff, 1997; Duan and Oglesby, 2005) of dynamic ruptures suggest in particular that slip is impeded and seismic rupture speed slows down on misoriented fault segments (Bouchon and Streiff, 1997; Duan and Oglesby, 2005), *i.e.*, segments unfavorably oriented with respect to the regional stress field and therefore with large strength excess (a large strength excess, defined as the difference between static frictional strength and initial shear stress, means that the pre-seismic stress is far from the condition for yielding). Seismically activated fault planes tend to be optimally oriented, in agreement with Anderson's theory of faulting: focal mechanims of shallow crustal earthquakes show dominanly either dip-slip or strike-slip sources, while sources with oblique slip are relatively rare (Celerier, 2008) (the zero shear stress at the Earth surface implies that one principal stress is vertical).

Both the shallow dip angle and the increasing the westward bend of the fault trace should make the Hosbah fault very unfavorably oriented for a strike-slip rupture. Nevertheless, the increase in high frequency radiation, as well as surface deformation and the finite source model all consistently show that the seismic rupture was actually boosted and not inhibited as it propagated along the fault bend. The rupture did not slow down either. The fact that the rupture could propagate over a long distance and with a speed close to that of the S-waves (see Table S1 for velocity structure) requires a small strength excess (Andrews, 1976) which is unexpected on a misoriented fault. In any case, the dynamic stress probably governed seismic fault slip favoring strike-slip motion over the thrust component that would be expected if the rupture had been driven only by the regional tectonic pre-stress field.

The Balochistan earthquake demonstrates that large ruptures can develop on severely misoriented faults and that dynamic stresses can induce large slip with a rake inconsistent with the pre-earthquake stress field. These characteristics require a low strength excess possibly attesting to an intrisically low yielding strength and/or very strong dynamic weakening. Interestingly, our source model shows slip increasing gradually upward to reach its maximum at the surface. This observation is in constrast with the near surface slip deficit which seems to characterize strike-slip earthquakes(Fialko et al., 2005), but is more alike the pattern observed in thrust earthquakes(Avouac et al., 2006; Ji et al., 2003) for which near surface large slip is potentially promoted by the interaction of the earthquake-generated stress field with Earth's free surface(Kozdon and Dunham, 2013; Oglesby et al., 1998; Oglesby and Day, 2001). This mechanism may have been at play during the 2013 Balochistan earthquake.

Our finding that the rupture propagated at an average speed nearly as fast as S waves also warrants explanation. Dynamic rupture models in homogeneous media predict that stable ruptures are either slower than Rayleigh waves (less than 92% of S speed) or significantly (more than 33%) faster than S waves (Andrews, 1976; Obrezanova and Willis, 2003) while speeds near the S wave speed are short-lived. It is possible that the rupture during he Balochistan was supershear intermittently, with speed fluctuations over length scales that our observations cannot resolve, leading to an average rupture speed near the S-waves velocity. However, the presence of a zone of compliant, damaged rock surrounding the fault provides a mechanism that does not require such ad hoc rupture complexity. Indeed, steady ruptures at speeds near the S wave of the undamaged crust result if the rupture is supershear with respect to the damaged rock (Huang et al., submitted; Huang and Ampuero, 2011) and seismic wave speeds inside the fault zone are 58% to 75% those of the host rock. Moreover, supershear ruptures in damaged fault zones are possible at lower background stresses than in homogeneous media (Huang et al., submitted). Compliance of the fault zone could thus explain how high rupture velocity was achieved on a mis-oriented fault. In any case, the Balochistan earthquake will serve as a good case-example to test dynamic models of rupture propagation on non planar-faults in the future.

Conclusion

This study illustrates the benefit of combining remote sensing of surface deformation with backprojection and finite source modeling of teleseismic waveforms to derive well constrained earthquake source models. The Balochistan earthquake is a rare example of large strike-slip motion on a low angle dipping fault. This kinematics must have resulted from reactivation of a fault which originally formed as a thrust fault within the Makran accretionnary prism. The reactivation was made possible due to the vertical axis bending of the thrust belt associated with left-lateral shear along the Chaman fault system. This case example is of particular interest to test dynamics models of seismic ruptures.

References

Ader, T., Avouac, J.P., Liu-Zeng, J., Lyon-Caen, H., Bollinger, L., Galetzka, J., Genrich, J., Thomas, M., Chanard, K., Sapkota, S.N., Rajaure, S., Shrestha, P., Ding, L., Flouzat, M., 2012. Convergence rate across the Nepal Himalaya and interseismic coupling on the Main Himalayan Thrust: Implications for seismic hazard. Journal of Geophysical Research-Solid Earth 117.

Ambraseys, N.N.a.B., R., 2003. Earthquakes and Associated Deformation in Northern Baluchistan. B. Seismol. Soc. Am. 93, 1573-1605.

Andrews, D.J., 1976. Rupture velocity of plane strain shear cracks. Journal of Geophysical Research 81, 5679-5687.

Avouac, J.P., Ayoub, F., Leprince, S., Konca, O., Helmberger, D.V., 2006. The 2005, M-w 7.6 Kashmir earthquake: Sub-pixel correlation of ASTER images and seismic waveforms analysis. Earth and Planetary Science Letters 249, 514-528.

Bouchon, M., Campillo, M., Cotton, F., 1998. Stress field associated with the rupture of the 1992 Landers, California, earthquake and its implications concerning the fault strength at the onset of the earthquake. Journal of Geophysical Research-Solid Earth 103, 21091-21097.

Bouchon, M., Streiff, D., 1997. Propagation of a shear crack on a nonplanar fault: A method of calculation. Bulletin of the Seismological Society of America 87, 61-66.

Bouchon, M., Toksoz, N., Karabulut, H., Bouin, M.P., Dietrich, M., Aktar, M., Edie, M., 2000. Seismic imaging of the 1999 Izmit (Turkey) rupture inferred from the near-fault recordings. Geophysical Research Letters 27, 3013-3016.

Byrne, D.E., Sykes, L.R., Davis, D.M., 1992. Great thrust earthquakes and aseismic slip along the plate boundary of the Makran subduction zone. Journal of Geophysical Research-Solid Earth 97, 449-478.

Celerier, B., 2008. Seeking Anderson's faulting in seismicity: A centennial celebration. Reviews of Geophysics 46.

Duan, B.C., Oglesby, D.D., 2005. Multicycle dynamics of nonplanar strike-slip faults. Journal of Geophysical Research-Solid Earth 110.

Ellouz-Zimmermann, N., Deville, E., Mueller, C., Lallemant, S., Subhani, A.B., Tabreez, A.R., 2007. Impact of sedimentation on convergent margin tectonics: Example of the Makran accretionary prism (Pakistan).

Fialko, Y., Sandwell, D., Simons, M., Rosen, P., 2005. Three-dimensional deformation caused by the Bam, Iran, earthquake and the origin of shallow slip deficit. Nature 435, 295-299.

Heaton, T.H., 1990. Evidence for and implications of self-healing pulses of slip in earthquake rupture. Physics of the Earth and Planetary Interiors 64, 1-20.

Huang, Y., Ampuero, J.-P., Helmberger, D.V., submitted. Earthquake ruptures modulated by waves in damaged fault zones. J. Geoph. Res.

Huang, Y.H., Ampuero, J.P., 2011. Pulse-like ruptures induced by low-velocity fault zones. Journal of Geophysical Research-Solid Earth 116.

Ishii, M., Shearer, P.M., Houston, H., Vidale, J.E., 2005. Extent, duration and speed of the 2004 Sumatra-Andaman earthquake imaged by the Hi-Net array. Nature 435, 933-936.

Ji, C., Helmberger, D.V., Wald, D.J., Ma, K.F., 2003. Slip history and dynamic implications of the 1999 Chi-Chi, Taiwan, earthquake. Journal of Geophysical Research-Solid Earth 108.

Ji, C., Wald, D., Helmberger, D.V., 2002. Source Description of the 1999 Hector Mine, California Earthquake, Part I: Wavelet Domain Inversion Theory and Resolution Analysis. Bull. Seismol. Soc. Am. 92, 1192-1207.

Kaneko, Y., Avouac, J.P., Lapusta, N., 2010. Towards inferring earthquake patterns from geodetic observations of interseismic coupling. Nature Geoscience 3, 363-U324.

Kase, Y., Day, S.M., 2006. Spontaneous rupture processes on a bending fault. Geophysical Research Letters 33.

King, G.C., Nabelek, J., 1985. The role of fault bends in faults in the initiation and termination of earthquake rupture. Science 283, 984-987.

Konca, A.O., Kaneko, Y., Lapusta, N., Avouac, J.P., 2013. Kinematic Inversion of Physically Plausible Earthquake Source Models Obtained from Dynamic Rupture Simulations. Bulletin of the Seismological Society of America 103, 2621-2644.

Kozdon, J.E., Dunham, E.M., 2013. Rupture to the Trench: Dynamic Rupture Simulations of the 11 March 2011 Tohoku Earthquake. Bulletin of the Seismological Society of America 103, 1275-1289.

Kukowski, N., Schillhorn, T., Flueh, E.R., Huhn, K., 2000. Newly identified strike-slip plate boundary in the northeastern Arabian Sea. Geology 28, 355-358.

Lawrence R.D., Khan S.H., Dejong K.A., A., F., Yeats R.S., 1981. Thrust and strike slip fault interaction along the Chaman transform zone, Pakistan. In:Thrust and Nappe tectonics., in: London, T.G.S.o. (Ed.), Thrust and Nappe tectonics., pp. 363–370.

Leprince, S., Barbot, S., Ayoub, F., Avouac, J.P., 2007. Automatic and precise orthorectification, coregistration, and subpixel correlation of satellite images, application to ground deformation measurements. Ieee Transactions on Geoscience and Remote Sensing 45, 1529-1558.

Meng, L.S., Inbal, A., Ampuero, J.P., 2011. A window into the complexity of the dynamic rupture of the 2011 Mw 9 Tohoku-Oki earthquake. Geophysical Research Letters 38.

Obrezanova, O., Willis, J.R., 2003. Stability of intersonic shear crack propagation. Journal of the Mechanics and Physics of Solids 51, 1957-1970.

Oglesby, D.D., Archuleta, R.J., Nielsen, S.B., 1998. Earthquakes on dipping faults: The effects of broken symmetry. Science 280, 1055-1059.

Oglesby, D.D., Day, S.M., 2001. Fault geometry and the dynamics of the 1999 Chi-Chi (Taiwan) earthquake. Bulletin of the Seismological Society of America 91, 1099-1111.

Platt, J.P., Leggett, J.K., Alam, S., 1988. Slip vectors and fault mechanics in the Makran accretionnary wedge, southwest Pakistan. Journal of Geophysical Research-Solid Earth and Planets 93, 7955-7973.

Reilinger, R., McClusky, S., Vernant, P., Lawrence, S., Ergintav, S., Cakmak, R., Ozener, H., Kadirov, F., Guliev, I., Stepanyan, R., Nadariya, M., Hahubia, G., Mahmoud, S., Sakr, K., ArRajehi, A., Paradissis, D., Al-Aydrus, A., Prilepin, M., Guseva, T., Evren, E., Dmitrotsa, A., Filikov, S.V., Gomez, F., Al-Ghazzi, R., Karam, G., 2006. GPS constraints on continental deformation in the Africa-Arabia-Eurasia continental collision zone and implications for the dynamics of plate interactions. Journal of Geophysical Research-Solid Earth 111.

Smith, G.L., McNeill, L.C., Wang, K.L., He, J.H., Henstock, T.J., 2013. Thermal structure and megathrust seismogenic potential of the Makran subduction zone. Geophysical Research Letters 40, 1528-1533.

Szeliga, W., Bilham, R., Kakar, D.M., Lodi, S.H., 2012. Interseismic strain accumulation along the western boundary of the Indian subcontinent. Journal of Geophysical Research-Solid Earth 117.